

Conservation laws and slow dynamics determine the universality class of interfaces in active matter

Raphaël Maire,^{1,*} Andrea Plati,¹ Frank Smallenburg,¹ and Giuseppe Foffi^{1,†}

¹*Université Paris-Saclay, CNRS, Laboratoire de Physique des Solides, 91405 Orsay, France*

(Dated: November 25, 2025)

While equilibrium interfaces display universal large-scale statistics, interfaces in phase-separated active and driven systems are predicted to belong to distinct non-equilibrium universality classes. Yet, such behavior has proven difficult to observe, with most systems exhibiting equilibrium-like fluctuations despite their strongly non-equilibrium microscopic dynamics. We introduce an active hard-disk model that contrary to self-propelled models, displays clear non-equilibrium interfacial scaling and observe for the first time, the $|\mathbf{q}|$ KPZ and wet- $|\mathbf{q}|$ KPZ universality classes while revealing a new, previously overlooked universality class arising in systems with slow crystalline or glassy dynamics. These distinct classes are selected by conservation laws and slow hydrodynamic modes.

Introduction - At thermodynamic equilibrium, the Boltzmann distribution governs all static observables [1]. For example, every liquid–gas critical point – whether in a colloidal suspension, a molecular fluid, or the μVT ensemble – shares the same static critical exponents [2] while the dynamics are captured by different dynamical exponents z [3, 4]. Similarly, interfaces in equilibrium phase-separated systems – such as those found in liquid–liquid colloid demixing [5], polymer blends [6], electrolyte solutions [7], or 2D Ising models [8] – are all governed by the capillary-wave Hamiltonian on large scales with surface tension γ : $\mathcal{H}[h] \simeq \frac{\gamma}{2} \int d^d x (\nabla h)^2$, where $h(\mathbf{x}, t)$ is the height of a d -dimensional interface [9]. Dynamically, projection methods show that the Fourier components $h(\mathbf{k}, t)$ evolve as [9–17]:

$$\partial_t h(\mathbf{k}, t) = -\kappa |\mathbf{k}|^{\alpha-2} \frac{\delta \mathcal{H}}{\delta h} + \sqrt{2\kappa |\mathbf{k}|^{\alpha-2} D} \zeta(\mathbf{k}, t), \quad (1)$$

where D is proportional to the temperature, $\zeta(\mathbf{k}, t)$ is a unit-variance Gaussian white noise, and $\kappa |\mathbf{k}|^{\alpha-2}$ is a damping. The dynamical exponent z characterizing the interface relaxation time equals α which depends on the conservation laws of the underlying $(d+1)$ -dimensional order parameter dynamics [12]. The fluctuation dissipation theorem ensures that static properties quantified by the static height correlation $S_h(\mathbf{k}) \equiv \langle |h(\mathbf{k})|^2 \rangle \sim \mathbf{k}^{-d-2\chi}$ with $\chi = (2-d)/2$, are independent of z at equilibrium [9]. This decoupling between statics and dynamics, is however only guaranteed at equilibrium.

With the rise of interest in active matter [18–20] and the ubiquity of interfaces in biology [21–27], research on far-from equilibrium interfaces has surged. In this work, we focus not on growing interfaces, such as those described by KPZ [28, 29], which make up a large class of physical systems, but rather on non-growing interfaces in phase-separated systems. Freed from a Hamiltonian framework, these interfaces can exhibit peculiar behavior such as negative surface tension [20, 30–32], instabilities [9, 33–36], and traveling waves [37–40]. These effects can typically be captured either by introducing effective parameters into the equilibrium interface equa-

tion (Eq. (1)) or by coupling this equation to another field. Surprisingly, the measured fluctuations in granular or scalar active matter interfaces often follow the equilibrium result: $S \sim |\mathbf{k}|^{-2}$ [41–52]. This equilibrium-like behavior remains puzzling. While microscopic violations of detailed balance do not always survive coarse-graining in other systems [53–60], theoretical predictions for interfaces in active matter, suggest a rich variety of non-equilibrium behaviors depending on the conserved quantity of the underlying dynamics. For example, in overdamped systems, such as active Brownian particles, the interface is predicted to obey the $|\mathbf{q}|$ KPZ equation [61, 62]:

$$\partial_t h = -\kappa \gamma |\mathbf{k}|^3 + \lambda |\mathbf{k}| \mathcal{F} [(\nabla h)^2] + \sqrt{2\kappa |\mathbf{k}| D} \zeta, \quad (2)$$

where \mathcal{F} denotes the Fourier transform and λ controls the non-linearity strength. Despite extensive researches in interfacial fluctuations of active matter interfaces [41–48, 52], $|\mathbf{q}|$ KPZ has been reported only once in numerical simulations of strongly confined active particles [63]. This scarcity of observation likely reflects that the universal regime emerges only at system sizes orders of magnitude larger than the persistence length. Including momentum conservation should yield the wet- $|\mathbf{q}|$ KPZ equation [64]:

$$\partial_t h = -\kappa \gamma |\mathbf{k}| + \lambda |\mathbf{k}|^{-1} \mathcal{F} [(\nabla h)^2] + \sqrt{2\kappa |\mathbf{k}|^{-1} D} \zeta, \quad (3)$$

which remains unobserved. Finally, for some non-equilibrium hyperuniform (HU) systems with momentum-conserving noise but non-conserving deterministic dynamics [65–67], the interface obeys:

$$\partial_t h = -\kappa \gamma |\mathbf{k}|^3 + \sqrt{2\kappa |\mathbf{k}|^2 D} \zeta. \quad (4)$$

To date, only this last equation has been clearly observed numerically in large-scale systems [68].

For 1D interfaces, each of these cases have different ex-

ponents:

1D interface		χ	z	Ref
Equilibrium	Eq. (1)	1/2	α	9
$ \mathbf{q} $ KPZ	Eq. (2)	0.3 – 0.4	2.2 – 2.8	61, 64
wet- $ \mathbf{q} $ KPZ	Eq. (3)	1	1	64
HU interface	Eq. (4)	0	3	68

Thus, three predicted non-equilibrium phase-separating models with distinct dynamics yield different static roughness exponents, breaking equilibrium universality.

The contribution of this work is twofold. (i) We introduce an active hard-disk model, inspired by a vibrated granular system which, in contrast to regular self-propelled active matter, exhibits clearly and for the first time all three non-equilibrium universality classes theoretically predicted for interfaces separating coexisting liquid and gas phases. (ii) We show that the emergence of crystallization or glassiness in one of the phases qualitatively modifies interfacial fluctuations, leading to new, previously overlooked universality classes. Taken together, these results reveal how conservation laws and slow relaxation processes can fundamentally reshape the static properties of interfaces in active matter systems.

Model - Taking inspiration from a granular system [69, 70], we model N 2D hard disks of mass m and diameter σ in a periodic $L_x \times L_y$ box at packing fraction $\phi = N\pi\sigma^2/(4L_xL_y)$. Each particle i follows the Langevin equation:

$$m \frac{d^2 \mathbf{r}_i}{dt^2} = -m\Gamma \frac{d\mathbf{r}_i}{dt} + \sum_{j \neq i} \mathbf{F}_{ij}^{\text{coll}} + \sqrt{2m\Gamma T} \zeta_i(t), \quad (5)$$

where Γ is a damping, T is a kinetic temperature, and $\mathbf{F}_{ij}^{\text{coll}}$ acts as a momentum-conserving non-equilibrium collision such that at contact ($|\mathbf{r}_i - \mathbf{r}_j| = \sigma$), the kinetic energy of i and j changes by [68, 71]:

$$\Delta E_{ij} = \Delta E_{ij}^+ - m \frac{1 - \alpha^2}{4} (\mathbf{v}_{ij} \cdot \hat{\boldsymbol{\sigma}}_{ij})^2, \quad (6)$$

with $\mathbf{v}_{ij} = \mathbf{v}_i - \mathbf{v}_j$, $\hat{\boldsymbol{\sigma}}_{ij} = (\mathbf{r}_i - \mathbf{r}_j)/\sigma$, and $0 \leq \alpha \leq 1$ a coefficient of restitution. If $\Gamma = 0$, we set $\alpha < 1$ to dissipate the energy injected by $\Delta E_{ij}^+ > 0$. The injected energy depends on the times since each particle's last collision τ_i and τ_j :

$$\Delta E_{ij}^+ = 2\delta E_0 + \delta E \left(1 - e^{-\tau_i/\tau_r}\right)^\beta + \delta E \left(1 - e^{-\tau_j/\tau_r}\right)^\beta, \quad (7)$$

where $2\delta E_0$ and $2(\delta E_0 + \delta E)$ are the minimal and maximal injections of energy interpolated in a time dependent on β and τ_r . For large δE , dense regions cool and compress while dilute regions heat and expand, destabilizing the homogeneous phase and driving phase separation with an interface separating the two phases [68, 71].

We perform hybrid time-stepped/event-driven molecular dynamics simulations [72] of Eqs. (5) and (6) in an elongated box ($L_x > L_y \equiv L$). Time and energy are measured in arbitrary units $\hat{\tau}$ and $\hat{E} = m(\sigma/\hat{\tau})^2/2$, respectively. The system is initialized with a step density profile along x at the coexistence densities of the two phases, and the interface position $h(y, t)$ is tracked over time (see Supplemental Material [73]).

Numerical results - The critical exponents are obtained from correlation functions starting from the flat interface of initial size L at $t = 0$ [74]:

$$W^2(L, t) \sim \begin{cases} L^{2\chi} & \text{if } t \gg \tau_{ss}(L) \\ t^{2\chi/z} & \text{if } t \ll \tau_{ss}(L) \end{cases}, \quad \tau_{ss}(L) \sim L^z \quad (8)$$

where $W^2 \equiv \langle (h(\mathbf{r}, t) - \langle h(\mathbf{r}, t) \rangle)^2 \rangle$ is the mean-squared width of the interface and τ_{ss} is the time required to reach a stationary state [73]. We will also use the static height correlation in the steady state $S_h(k) \equiv \langle |h(k)| \rangle \sim k^{-1-2\chi}$ in 1D. The simulation results are summarized in Fig. 1, with three limiting cases of our model shown in different rows.

(i) *$|\mathbf{q}|$ KPZ scaling.* In the top row ($T \neq 0$ and $\Gamma \neq 0$), the Langevin bath damps the momentum, leaving the density as the only conserved field. This should place the resulting interface in the $|\mathbf{q}|$ KPZ universality class where the following critical exponents are expected: $2.2 \lesssim z_{|\mathbf{q}|KPZ} \lesssim 2.8$ and $0.3 \lesssim \chi_{|\mathbf{q}|KPZ} \lesssim 0.4$. Panel a) shows a snapshot where the dense (left) region is colder, a strong non-equilibrium signature. The interface roughness is quantified in panel b) by the static height correlation $S_h(k) \sim k^{-1.5}$, yielding $\chi \simeq 0.25$. This roughness is significantly reduced compared to the equilibrium value $\chi^{\text{eq}} = 1/2$. Panel c) presents the time evolution of the interface width squared for various system sizes. During coarsening, we observe a slow growth of the interface width squared $W^2(t) \sim t^{0.18}$, incompatible with the equilibrium scaling $\sim t^{1/3}$. Combining this with $\chi \simeq 0.25$ yields a dynamical exponent $z \simeq 2\chi/0.18 \simeq 2.78$ via Eqs. (8). These exponents are confirmed in panel d) and e) which show respectively measurement of τ_{ss} and $W_{ss}^2 \equiv W^2(t \rightarrow \infty)$ as a function of L . Within finite-size limitations, our measured exponents are therefore consistent with the $|\mathbf{q}|$ KPZ scaling.

(ii) *wet- $|\mathbf{q}|$ KPZ scaling.* In the middle row ($\Gamma = 0$), the momentum is locally conserved due to the absence of a Langevin bath. This additional conservation law is expected to place the system in the wet- $|\mathbf{q}|$ KPZ universality class, characterized by $z^{\text{wet}} = 1$ and $\chi^{\text{wet}} = 1$. As shown in panel f), the interface is visibly rougher than in the previous case. This is quantified in panel g) and h), where $S_h(k) \sim k^{-3}$ and $W_{ss}^2 \sim L^2$ are found, both yielding $\chi \simeq 1$, consistent with theoretical expectations. The dynamics in panel h) and i), however, show deviation from standard coarsening behavior: the interface width does not exhibit clear power-law growth. This is

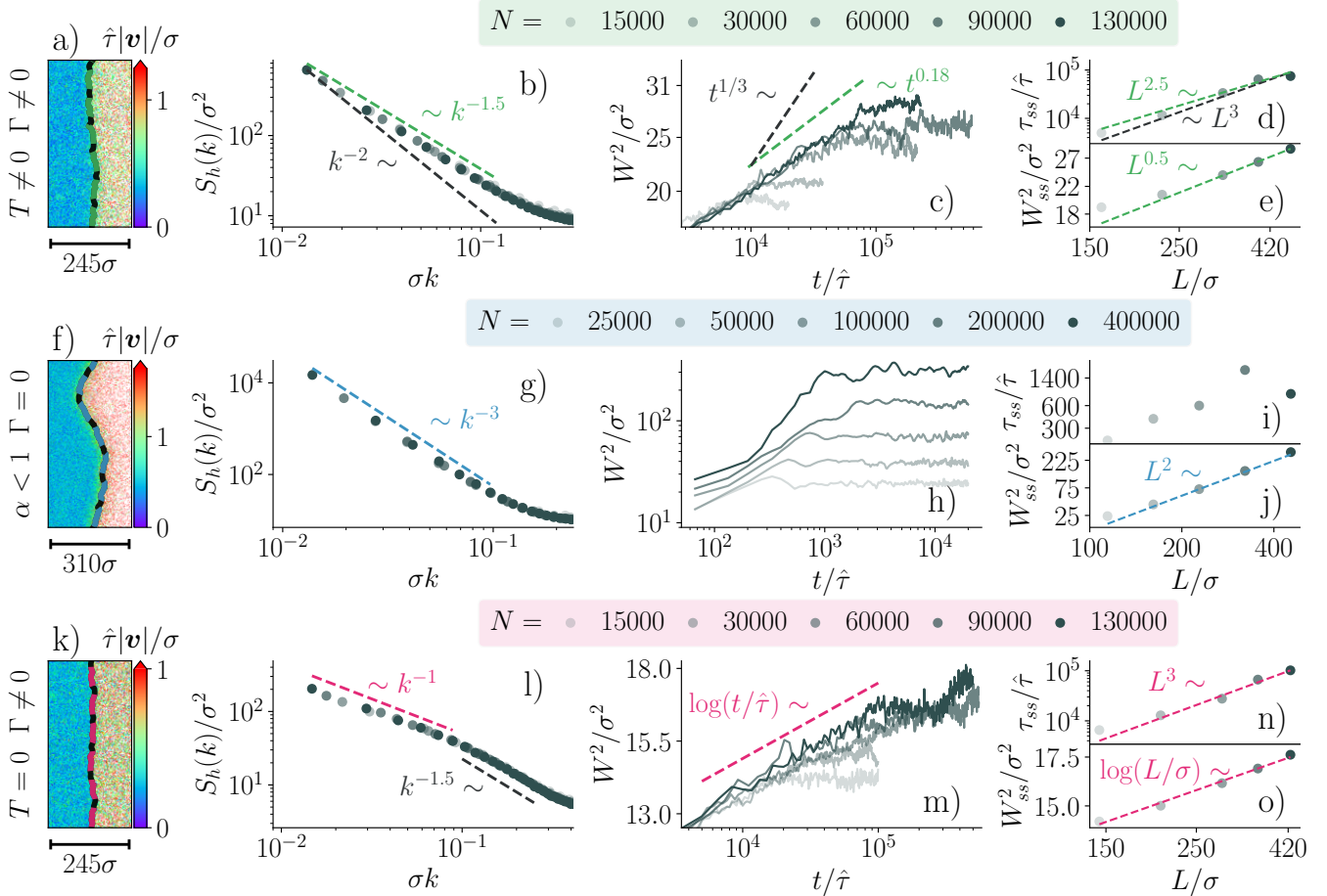


FIG. 1. Simulations of three qualitatively distinct systems based on Eqs. (5) and (6). In the first row, only the density field is conserved, in the second row, momentum is also conserved and in the last row only the density field is conserved but the mesoscopic noise conserves the center-of-mass of the system. a), f), and k) show snapshots centered on the interface, with particles colored by velocity. Panels b), g), and l) display the steady-state static height correlations as a function of wavenumber. c), h), and m) show the time evolution of the interface width squared, starting from a flat interface, for various system sizes. d), e), i), j), n), and o) show the system-size dependence of the coarsening time and steady-state width squared $W_{ss}^2 \equiv W^2(t \rightarrow \infty)$. The averages are computed over 50 to 1000 independent initial configurations, with at least 300 snapshots taken for each configuration. In a-e), we set $T/\hat{E} = 0.05$, $\Gamma/\hat{\tau} = 0.05$, $\tau_r/\hat{\tau} = 4$, $\delta E_0/\hat{E} = 0.0025$, $\delta E/\hat{E} = 15$, $\beta = 10$, $\alpha = 0.99$ and $L_x = 2L_y$. For f-j), we set $\Gamma/\hat{\tau} = 0$, $\tau_r/\hat{\tau} = 3$, $\delta E_0/\hat{E} = 0.0125$, $\delta E/\hat{E} = 25$, $\beta = 10$, $\alpha = 0.95$ and $L_x = 8L_y$. For k-o), we set $T/\hat{E} = 0$, $\Gamma/\hat{\tau} = 0.075$, $\tau_r/\hat{\tau} = 3$, $\delta E_0/\hat{E} = 0.0125$, $\delta E/\hat{E} = 25$, $\beta = 10$ and $\alpha = 0.95$, $L_x = 2L_y$.

consistent with direct simulation of the wet- $|\mathbf{q}|$ KPZ field equation, which reported an anomalous roughening [64]. Our simulations are also plagued by persistent oscillations (see Supplemental Material [73]). For these reasons, we do not try to investigate the typical coarsening time of this system.

(iii) *Hyperuniform scaling.* In the bottom row ($T = 0$ and $\Gamma \neq 0$), momentum is damped but still conserved by the collisions – the only source of activity. As shown in panel k), this leads to a very flat interface [68]. This is quantified in panel l), where the static height correlation scales as $S_h(k) \sim k^{-1}$, consistent with the theoretical prediction $\chi^{\text{HU}} = 0$ in $d = 1$. $\chi = 0$ implies that the interface width grows only logarithmically during coarsening (panel m), preventing a meaningful extraction of

z from early-time dynamics. Instead, we determine z from the relaxation time (panel n), obtaining $z \simeq 3$, in agreement with the theoretical prediction $z^{\text{HU}} = 3$. Finally, panel o) further confirms the vanishing roughness exponent, $\chi = 0$.

Liquid-solid interfaces — Having identified three universality classes for non-equilibrium liquid-gas interfaces, we now turn to non-equilibrium solid-liquid interfaces. While equilibrium 1D solid-liquid interfaces exhibit capillary-wave-like behavior [75], out of equilibrium, the slow relaxation of the phonons in the bulk of the crystal may modify the interface's static exponents. Such interfaces are particularly relevant for active matter, where even weak activity can induce crystallization [76–78].

A crystalline phase naturally emerges when the dense

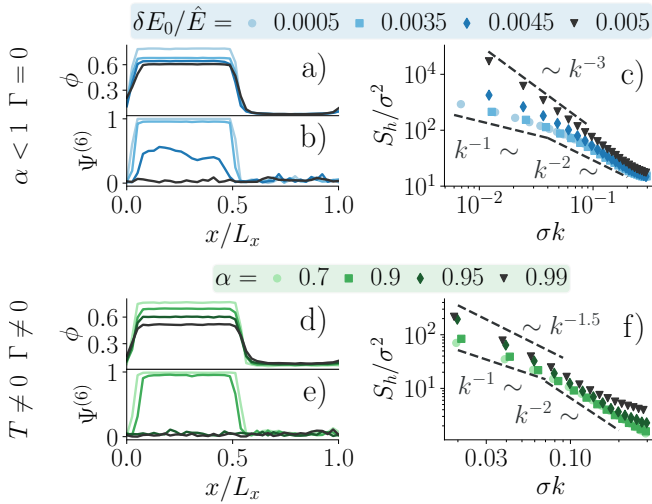


FIG. 2. Simulations of a liquid-solid interface in a system with momentum conservation (top) and without momentum conservation (bottom). a), d) and b), e) are the local packing fraction and bond orientational order profiles normal to the interface, respectively. c) and f) are the static height correlations with respect to the wavevector showing a scaling change when the dense phase crystallizes. The parameters, except the ones explicitly varied, are the same as in Fig. 1. For the system with $\Gamma = 0$, $N \simeq 2 \times 10^5$, for the other $N \simeq 8 \times 10^4$.

phase exceeds a packing fraction $\phi \gtrsim 0.7$. Such high packing fraction can be induced by tuning parameters ($\alpha \rightarrow 0$ or $\delta E_0 \rightarrow 0$) to make the dense phase effectively colder, promoting a tightly packed phase. Fig. 2 presents simulations of liquid-solid interfaces, focusing on their static properties (coarsening dynamics and finite size analysis are detailed in the Supplemental Material [73]). The top row corresponds to momentum conserving systems at various δE_0 , where wet- $|\mathbf{q}|$ KPZ scaling is expected for liquid-gas interfaces. Panel a) shows the local packing fraction profile in the direction normal to the interface. As expected, lowering δE_0 increases the dense phase packing. In panel b), we quantify crystallization using the bond-orientational order parameter, defined for each particle i as $\psi_i^{(6)} = \sum_j e^{-i6\theta_{ij}}$, where θ_{ij} is the angle between particle i , its neighbors j (with $|\mathbf{r}_i - \mathbf{r}_j| < 1.3\sigma$), and an arbitrary reference axis. At low δE_0 , $\Psi^{(6)} = N^{-1} |\sum_i \psi_i^{(6)}| \rightarrow 1$, indicating a well-ordered crystal. At higher δE_0 , the system remains disordered, and $\Psi^{(6)}$ remains small. For the intermediate case ($\delta E_0/\hat{E} = 0.0045$), the average bond-orientational parameter is reduced because contributions from slowly coarsening multiple hexatic domains partially cancel one another. In panel c), we show the interface fluctuations for these various systems. As expected, the system with a liquid dense phase follows the wet- $|\mathbf{q}|$ KPZ scaling $\chi \simeq 1$, but as the dense phase solidifies, the spectrum shifts toward $\chi \simeq 0$. In the bottom row of Fig. 2, we perform the same analysis but for a system without momentum

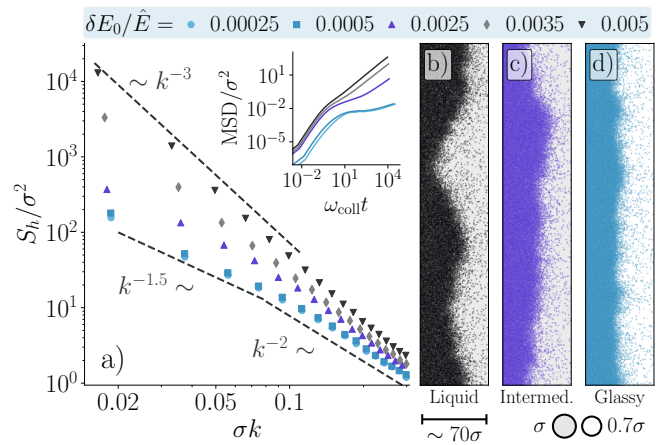


FIG. 3. Simulations of a liquid-glass interface in a binary hard-disk mixture with momentum conservation. a) Static height correlations versus wavevector show a change in scaling as the dense phase becomes glassy, as measured in the inset showing the mean-square displacement (MSD) of homogeneous systems at the corresponding dense-phase densities, plotted against time normalized by the collision rate ω_{coll} . b-d) Representative interface profiles for low, intermediate, and high δE_0 . All parameters match those in Fig. 1, except for the varied δE_0 and $\alpha = 0.9$. $2.5 \times 10^5 \leq N \leq 3.5 \times 10^5$. The mixture is equimolar with sizeratio 0.7.

conservation. As shown in panel f), when the system crystallizes (for $\alpha \leq 0.9$, as seen in panels d) and e)), the static height correlations deviate from the expected $|\mathbf{q}|$ KPZ scaling and $\chi \rightarrow 0$. This qualitatively mirrors the behavior observed in the momentum-conserving system. The system with center-of-mass conservation is also found to remain at $\chi = 0$. Thus, crystallization in the dense phase coincides with a universal shift of χ from its liquid-gas value to 0.

Liquid-glass interfaces — We now analyze liquid-glass interfaces which are highly relevant in biological systems [79–82]. Similar to crystallization, the slow dynamics of glasses and their low-energy excitations [83–85] may influence the static scaling of non-equilibrium interfaces. To suppress crystallization and enable liquid-glass coexistence, we replace the monodisperse system with a binary mixture of large and small hard particles, both governed by the same equations of motion. Denser phases are accessed by reducing the minimum injected energy $2\delta E_0$. Simulations for a momentum-conserving system are presented in Fig. 3a). At high δE_0 , the scaling exponent $\chi^{\text{wet}} = 1$ is recovered, as expected for an interface separating liquid and gas phases. However, as δE_0 is reduced, the dense phase undergoes dynamical arrest, evidenced by the plateau in the mean square displacement (inset). This coincides with a decrease of χ from 1 to 0.25. As expected, the resulting liquid-glass interface is visually less rough than the liquid-gas interface, with typical configurations shown in Fig. 3b-d). We thus find

a phenomenology consistent with that observed for solid-liquid interfaces: the interface roughness decreases when slow dynamics develop in the bulk of the dense phase.

Conclusion - We introduced a minimal active hard-disk model that realizes three distinct non-equilibrium liquid-gas universality classes of interfacial fluctuations, each tied to specific bulk conservation laws. We also uncovered that slow dynamics arising from crystallization or glassiness in the denser phase can modify the interface properties. This model directly maps onto quasi-2D vibrated granular systems undergoing phase separation, offering an experimentally accessible platform for probing non-equilibrium interfacial physics [70]. Unlike many active matter systems – where long persistence lengths and interfacial polarization might necessitate a large system to observe universal scaling [86–89] – this granular system may offer a more accessible path to asymptotic behavior.

To go beyond our studies, it would be valuable to develop a theory that predicts the measured interfacial exponents, specifically $\chi \simeq 0$ for liquid–solid interfaces and $\chi \simeq 0.25$ for liquid–glass interfaces. Building on the 1D flat interfaces studied here, exploring two-dimensional or curved interfaces – relevant for biological systems [24–27, 90–93], finite-size effects [41], and nucleation [94–98] – offers an interesting direction. For example, nucleation driven by active collisions may exhibit strong non-equilibrium behavior [99], distinct from that in conventional active matter [94]. More generally, interfaces with additional internal order (nematic, smectic, or polar) could reveal new universality classes, offering an exciting avenue for future study.

ACKNOWLEDGEMENTS

We gratefully acknowledge insightful discussions with Ludovic Berthier and Leonardo Galliano, as well as valuable exchanges with Adhvik Jaghannatan, Lila Sarfati, Julien Tailleur, Cesare Nardini, and Ananyo Maitra.

* raphael.maire@universite-paris-saclay.fr

† giuseppe.foffi@universite-paris-saclay.fr

- [1] M. Kardar, *Statistical physics of fields* (Cambridge University Press, 2007).
- [2] N. Goldenfeld, *Lectures on phase transitions and the renormalization group* (CRC Press, 2018).
- [3] G. Mazenko, *Nonequilibrium statistical mechanics* (John Wiley & Sons, 2006).
- [4] U. C. Täuber, *Critical dynamics: a field theory approach to equilibrium and non-equilibrium scaling behavior* (Cambridge University Press, 2014).
- [5] D. G. Aarts, M. Schmidt, and H. N. Lekkerkerker, Direct visual observation of thermal capillary waves, *Science* **304**, 847 (2004).
- [6] D. Langevin, Light scattering by liquid surfaces, new developments, *Adv. Colloid Interfac.* **289**, 102368 (2021).
- [7] M. Safouane and D. Langevin, Surface viscoelasticity of concentrated salt solutions: specific ion effects, *ChemPhysChem* **10**, 222 (2009).
- [8] G. Gallavotti, The phase separation line in the two-dimensional ising model, *Commun. Math. Phys.* **27**, 103 (1972).
- [9] A. Onuki, *Phase transition dynamics* (Cambridge University Press, 2002).
- [10] K. Kawasaki and T. Ohta, Kinetic drumhead model of interface. i, *Prog. Theor. Phys.* **67**, 147 (1982).
- [11] R. I. Slavchov, B. Peychev, and A. S. Ismail, Characterization of capillary waves: A review and a new optical method, *Phys. Fluids* **33** (2021).
- [12] A. J. Bray, A. Cavagna, and R. D. Travasso, Interface fluctuations, burgers equations, and coarsening under shear, *Phys. Rev. E* **65**, 016104 (2001).
- [13] R. Bausch, V. Dohm, H. Janssen, and R. Zia, Critical dynamics of an interface in $1+\epsilon$ dimensions, *Phys. Rev. Lett.* **47**, 1837 (1981).
- [14] R. Zia, Normal coordinates and curvature terms in an interface hamiltonian, *Nucl. Phys. B* **251**, 676 (1985).
- [15] R. Zia, R. Bausch, H. Janssen, and V. Dohm, Dynamics of an interface coupled to a diffusive bulk mode, *Mod. Phys. Lett. B* **2**, 961 (1988).
- [16] J. Romano, R. Golestanian, and B. Mahault, Dynamics of phase-separated interfaces in inhomogeneous and driven mixtures, *Soft Matter* (2025).
- [17] N. Caballero, E. Agoritsas, V. Lecomte, and T. Giarmarchi, From bulk descriptions to emergent interfaces: Connecting the ginzburg-landau and elastic-line models, *Phys. Rev. B* **102**, 104204 (2020).
- [18] M. Te Vrugt and R. Wittkowski, Metareview: a survey of active matter reviews, *Eur. Phys. J. E* **48**, 12 (2025).
- [19] M. C. Marchetti, J.-F. Joanny, S. Ramaswamy, T. B. Liverpool, J. Prost, M. Rao, and R. A. Simha, Hydrodynamics of soft active matter, *Reviews of modern physics* **85**, 1143 (2013).
- [20] M. E. Cates and C. Nardini, Active phase separation: new phenomenology from non-equilibrium physics, *Rep. Progr. Phys.* **88**, 056601 (2025).
- [21] R. A. Foty and M. S. Steinberg, The differential adhesion hypothesis: a direct evaluation, *Developmental biology* **278**, 255 (2005).
- [22] A. A. Hyman, C. A. Weber, and F. Jülicher, Liquid-liquid phase separation in biology, *Annual review of cell and developmental biology* **30**, 39 (2014).
- [23] S. C. Kammeraat, Y.-E. Keta, P. Appleton, I. P. Newton, T. B. Liverpool, R. Sknepnek, I. Näthke, and S. Henkes, Correlated cell movements drive epithelial finger formation, [arXiv:2508.01046](https://arxiv.org/abs/2508.01046) (2025).
- [24] B. Schamberger, R. Ziege, K. Anselme, M. Ben Amar, M. Bykowski, A. P. Castro, A. Cipitria, R. A. Coles, R. Dimova, M. Eder, *et al.*, Curvature in biological systems: its quantification, emergence, and implications across the scales, *Adv. Mater.* **35**, 2206110 (2023).
- [25] B. R. Sabari, A. Dall’Agnese, and R. A. Young, Biomolecular condensates in the nucleus, *Trends in biochemical sciences* **45**, 961 (2020).
- [26] C. P. Brangwynne, C. R. Eckmann, D. S. Courson, A. Rybarska, C. Hoege, J. Gharakhani, F. Jülicher, and A. A. Hyman, Germline p granules are liquid droplets that localize by controlled dissolution/condensation,

- Science* **324**, 1729 (2009).
- [27] A. Molliex, J. Temirov, J. Lee, M. Coughlin, A. P. Kana-
garaj, H. J. Kim, T. Mittag, and J. P. Taylor, Phase
separation by low complexity domains promotes stress
granule assembly and drives pathological fibrillization,
Cell **163**, 123 (2015).
- [28] M. Kardar, G. Parisi, and Y.-C. Zhang, Dynamic scaling
of growing interfaces, *Phys. Rev. Lett.* **56**, 889 (1986).
- [29] K. A. Takeuchi and M. Sano, Universal fluctuations of
growing interfaces: evidence in turbulent liquid crystals,
Physical review letters **104**, 230601 (2010).
- [30] J. Bialké, J. T. Siebert, H. Löwen, and T. Speck, Nega-
tive interfacial tension in phase-separated active brown-
ian particles, *Physical review letters* **115**, 098301 (2015).
- [31] G. Fausti, E. Tjhung, M. Cates, and C. Nardini, Capil-
lary interfacial tension in active phase separation, *Phys-
ical review letters* **127**, 068001 (2021).
- [32] R. Singh and M. Cates, Hydrodynamically interrupted
droplet growth in scalar active matter, *Physical review
letters* **123**, 148005 (2019).
- [33] L. Zhao, P. Gulati, F. Caballero, I. Kolvin, R. Adkins,
M. C. Marchetti, and Z. Dogic, Asymmetric fluctuations
and self-folding of active interfaces, *Proc. Natl. Acad.
Sci.* **121** (2024).
- [34] R. Alert, Fingering instability of active nematic
droplets, *Journal of Physics A: Mathematical and The-
oretical* **55**, 234009 (2022).
- [35] R. Adkins, I. Kolvin, Z. You, S. Witthaus, M. C.
Marchetti, and Z. Dogic, Dynamics of active liquid in-
terfaces, *Science* **377**, 768 (2022).
- [36] A. Martínez-Calvo, C. Trenado-Yuste, H. Lee, J. Gore,
N. S. Wingreen, and S. S. Datta, Interfacial morphody-
namics of proliferating microbial communities, *Physical
Review X* **15**, 011016 (2025).
- [37] P. Gulati, F. Caballero, I. Kolvin, Z. You, and M. C.
Marchetti, Traveling waves at the surface of active liquid
crystals, *Soft Matter* **20**, 7703 (2024).
- [38] P. Barthelet and F. Charru, Benjamin-feir and eckhaus
instabilities with galilean invariance: the case of inter-
facial waves in viscous shear flows, *European Journal of
Mechanics-B* **17**, 1 (1998).
- [39] L. Langford and A. K. Omar, Phase separation, capil-
larity, and odd-surface flows in chiral active matter,
Phys. Rev. Lett. **134**, 068301 (2025).
- [40] F. Raßhofer, S. Bauer, A. Ziepke, I. Maryshev, and
E. Frey, Capillary wave formation in conserved active
emulsions, [arXiv:2505.20028](https://arxiv.org/abs/2505.20028) (2025).
- [41] L.-H. Luu, G. Castillo, N. Mujica, and R. Soto, Capil-
lary like fluctuations of a solid-liquid interface in a
noncohesive granular system, *Phys. Rev. E* **87**, 040202
(2013).
- [42] L. Yao and R. L. Jack, Interfacial and density fluctua-
tions in a lattice model of motility-induced phase separa-
tion, *J. Chem. Phys.* **162**, 114902 (2025).
- [43] A. Wysocki, R. G. Winkler, and G. Gompper, Propagat-
ing interfaces in mixtures of active and passive brownian
particles, *New J. Phys.* **18**, 123030 (2016).
- [44] L. Langford and A. K. Omar, Theory of capillary
tension and interfacial dynamics of motility-induced
phases, *Phys. Rev. E* **110**, 054604 (2024).
- [45] A. Patch, D. M. Sussman, D. Yllanes, and M. C.
Marchetti, Curvature-dependent tension and tangential
flows at the interface of motility-induced phases, *Soft
matter* **14**, 7435 (2018).
- [46] C. F. Lee, Interface stability, interface fluctuations,
and the gibbs–thomson relationship in motility-induced
phase separations, *Soft matter* **13**, 376 (2017).
- [47] S. Paliwal, V. Prymidis, L. Filion, and M. Dijkstra,
Non-equilibrium surface tension of the vapour-liquid in-
terface of active lennard-jones particles, *The Journal of
chemical physics* **147**, 084902 (2017).
- [48] C. Del Junco and S. Vaikuntanathan, Interface height
fluctuations and surface tension of driven liquids with
time-dependent dynamics, *J. Chem. Phys.* **150**, 094708
(2019).
- [49] Z. Sun, L. Li, F. Ye, and M. Yang, Interfacial stability
in tensionless phase-separated quorum-sensing systems,
[arXiv:2507.15030](https://arxiv.org/abs/2507.15030) (2025).
- [50] A. E. Patteson, A. Gopinath, and P. E. Arratia, The
propagation of active-passive interfaces in bacterial
swarms, *Nature communications* **9**, 5373 (2018).
- [51] R. C. Coelho, N. A. Araújo, and M. M. T. da Gama,
Propagation of active nematic–isotropic interfaces on
substrates, *Soft Matter* **16**, 4256 (2020).
- [52] E. Chacón, F. Alarcón, J. Ramírez, P. Tarazona, and
C. Valeriani, Intrinsic structure perspective for mips in-
terfaces in two-dimensional systems of active brownian
particles, *Soft Matter* **18**, 2646 (2022).
- [53] G. G. Lorenzana, D. Martin, Y. Avni, D. S. Seara,
M. Fruchart, G. Biroli, and V. Vitelli, When is non-
reciprocity relevant?, [arXiv:2509.17972](https://arxiv.org/abs/2509.17972) (2025).
- [54] N. Papanikolaou and T. Speck, Dynamic renormaliza-
tion of scalar active field theories, [arXiv:2404.09999](https://arxiv.org/abs/2404.09999)
(2024).
- [55] F. Caballero and M. E. Cates, Stealth entropy produc-
tion in active field theories near ising critical points,
Phys. Rev. Lett. **124**, 240604 (2020).
- [56] J. O’Byrne, Y. Kafri, J. Tailleur, and F. van Wijland,
Time irreversibility in active matter, from micro to
macro, *Nature Reviews Physics* **4**, 167 (2022).
- [57] A. Plati, R. Maire, F. Boulogne, F. Restagno, F. Small-
enburg, and G. Foffi, Self-assembly and non-equilibrium
phase coexistence in a binary granular mixture, *J.
Chem. Phys.* **163** (2025).
- [58] A. Crisanti, A. Puglisi, and D. Villamaina, Nonequilib-
rium and information: The role of cross correlations,
Phys. Rev. E **85**, 061127 (2012).
- [59] É. Fodor, R. L. Jack, and M. E. Cates, Irreversibility
and biased ensembles in active matter: Insights from
stochastic thermodynamics, *Annu. Rev. Condens. Ma-
t. P.* **13**, 215 (2022).
- [60] D. Lucente, A. Baldassarri, A. Puglisi, A. Vulpiani, and
M. Viale, Inference of time irreversibility from incom-
plete information: Linear systems and its pitfalls, *Phys.
Rev. Res.* **4**, 043103 (2022).
- [61] M. Besse, G. Fausti, M. E. Cates, B. Delamotte,
and C. Nardini, Interface roughening in nonequilibrium
phase-separated systems, *Phys. Rev. Lett.* **130**, 187102
(2023).
- [62] J. Toner, Roughening of two-dimensional interfaces in
nonequilibrium phase-separated systems, *Phys. Rev. E*
107, 044801 (2023).
- [63] B. Krishan, Finite size scaling and universality classes
of one-dimensional active matter interface, *Europhys.
Lett.* **150**, 37003 (2025).
- [64] F. Caballero, A. Maitra, and C. Nardini, Interface dy-
namics of wet active systems, *Phys. Rev. Lett.* **134**,

- 087105 (2025).
- [65] R. Maire and L. Chaix, Hyperuniformity and conservation laws in non-equilibrium systems, [arXiv:2509.04242 \(2025\)](#).
- [66] D. Hexner and D. Levine, Noise, diffusion, and hyperuniformity, *Phys. Rev. Lett.* **118**, 020601 (2017).
- [67] Y. Lei and R. Ni, Non-equilibrium dynamic hyperuniform states, *J. Phys. Condens. Matter* **37**, 023004 (2024).
- [68] R. Maire, L. Galliano, A. Plati, and L. Berthier, Hyperuniform interfaces in non-equilibrium phase coexistence, [arXiv:2507.03957 \(2025\)](#).
- [69] R. Maire, A. Plati, F. Smallenburg, and G. Foffi, Non-equilibrium coexistence between a fluid and a hotter or colder crystal of granular hard disks, *J. Chem. Phys.* **162**, 124901 (2025).
- [70] R. Maire, A. Plati, F. Smallenburg, and G. Foffi, Dynamical and structural properties of an absorbing phase transition: a case study from granular systems, [arXiv:2507.06083 \(2025\)](#).
- [71] D. Risso, R. Soto, and M. Guzmán, Effective two-dimensional model for granular matter with phase separation, *Phys. Rev. E* **98**, 022901 (2018).
- [72] F. Smallenburg, Efficient event-driven simulations of hard spheres, *Eur. Phys. J. E* **45**, 22 (2022).
- [73] See the Supplementary Material, which includes details on the numerical simulations and the coarsening analysis of the liquid-solid interfaces as well as Refs. 100 and 101.
- [74] F. Caballero, C. Nardini, F. van Wijland, and M. E. Cates, Strong coupling in conserved surface roughening: A new universality class?, *Phys. Rev. Lett.* **121**, 020601 (2018).
- [75] S. Safran, *Statistical thermodynamics of surfaces, interfaces, and membranes* (CRC Press, 2018).
- [76] A. K. Omar, K. Klymko, T. GrandPre, and P. L. Geissler, Phase diagram of active brownian spheres: Crystallization and the metastability of motility-induced phase separation, *Phys. Rev. Lett.* **126**, 188002 (2021).
- [77] D. Evans and A. K. Omar, Theory of nonequilibrium crystallization and the phase diagram of active brownian spheres, [arXiv:2411.14536 \(2024\)](#).
- [78] L. Caprini, D. Breoni, A. Ldov, C. Scholz, and H. Löwen, Dynamical clustering and wetting phenomena in inertial active matter, *Communications Physics* **7**, 343 (2024).
- [79] W. Kang, J. Ferruzzi, C.-P. Spatarelu, Y. L. Han, Y. Sharma, S. A. Koehler, J. A. Mitchel, A. Khan, J. P. Butler, D. Roblyer, *et al.*, A novel jamming phase diagram links tumor invasion to non-equilibrium phase separation, *Iscience* **24** (2021).
- [80] B. R. Parry, I. V. Surovtsev, M. T. Cabeen, C. S. O’hern, E. R. Dufresne, and C. Jacobs-Wagner, The bacterial cytoplasm has glass-like properties and is fluidized by metabolic activity, *Cell* **156**, 183 (2014).
- [81] A. Mongera, P. Rowghanian, H. J. Gustafson, E. Shelton, D. A. Kealhofer, E. K. Carn, F. Serwane, A. A. Lucio, J. Giammona, and O. Campàs, A fluid-to-solid jamming transition underlies vertebrate body axis elongation, *Nature* **561**, 401 (2018).
- [82] S. Sadhukhan, S. Dey, S. Karmakar, and S. K. Nandi, A perspective on active glassy dynamics in biological systems, *Eur. Phys. J. Special Topics* **233**, 3193 (2024).
- [83] P. M. Goldbart, Statistical field theory of equilibrium amorphous solids and the intrinsic heterogeneity distributions that characterize them, [arXiv:2505.14954 \(2025\)](#).
- [84] L. Gartner and E. Lerner, Nonlinear modes disentangle glassy and goldstone modes in structural glasses, *SciPost Phys.* **1**, 016 (2016).
- [85] Y.-C. Hu and H. Tanaka, Origin of the boson peak in amorphous solids, *Nat. Phys.* **18**, 669 (2022).
- [86] P. Pérez-Bastías and R. Soto, Two-field theory for phase coexistence of active brownian particles, *Phys. Rev. E* **112**, 10.1103/qlms-5wmd (2025).
- [87] L. Caprini, U. Marini Bettolo Marconi, and A. Puglisi, Spontaneous velocity alignment in motility-induced phase separation, *Phys. Rev. Lett.* **124**, 078001 (2020).
- [88] C. F. Lee, Active particles under confinement: aggregation at the wall and gradient formation inside a channel, *New J. Phys.* **15**, 055007 (2013).
- [89] S. Hermann and M. Schmidt, Active interface polarization as a state function, *Phys. Rev. Res.* **2**, 022003 (2020).
- [90] Y. Kuroda, T. Kawasaki, and A. M. Menzel, Effects of curvature on growing films of microorganisms, *Biophys. J.* **124**, 1609 (2025).
- [91] S. Hyde, Z. Blum, T. Landh, S. Lidin, B. Ninham, S. Andersson, and K. Larsson, *The language of shape: the role of curvature in condensed matter: physics, chemistry and biology* (Elsevier, 1996).
- [92] C. Liu, D. Cao, S. Liu, and Y. Wu, Nonequilibrium dynamics of membraneless active droplets (2025).
- [93] D. Zwicker, O. Paulin, and C. Ter Burg, Physics of droplet regulation in biological cells, *Reports on Progress in Physics* (2025).
- [94] M. E. Cates and C. Nardini, Classical nucleation theory for active fluid phase separation, *Phys. Rev. Lett.* **130**, 098203 (2023).
- [95] L. Langford and A. K. Omar, The mechanics of nucleation and growth and the surface tensions of active matter, *J. Chem. Phys.* **163** (2025).
- [96] R. Zakine, E. Simonnet, and E. Vanden-Eijnden, Unveiling the phase diagram and reaction paths of the active model b with the deep minimum action method, *Phys. Rev. Lett.* **133**, 038301 (2024).
- [97] D. Richard, H. Löwen, and T. Speck, Nucleation pathway and kinetics of phase-separating active brownian particles, *Soft Matter* **12**, 5257 (2016).
- [98] N. A. Sarma, D. A. King, X. Wu, B. A. Helms, P. D. Ashby, T. P. Russell, and A. K. Omar, Dynamic permeability in metastable droplet interfacial bilayers, [arXiv:2511.09510 \(2025\)](#).
- [99] R. Maire, Non-equilibrium systems driven by active collisions. *Section 4.6: Nucleating hyperuniform systems*, PhD Thesis (2025).
- [100] L. Ma, X. Li, and C. Liu, Fluctuation-dissipation theorem consistent approximation of the langevin dynamics model, *Commun. Math. Sci.* **15**, 1171 (2017).
- [101] F. Smallenburg, G. Del Monte, M. de Jager, and L. Filion, A simple and accurate method to determine fluid–crystal phase boundaries from direct coexistence simulations, *J. Chem. Phys.* **160** (2024).
- [102] M. Grant and R. C. Desai, Fluctuating hydrodynamics and capillary waves, *Phys. Rev. A* **27**, 2577 (1983).

Supplemental Material

Simulation methods

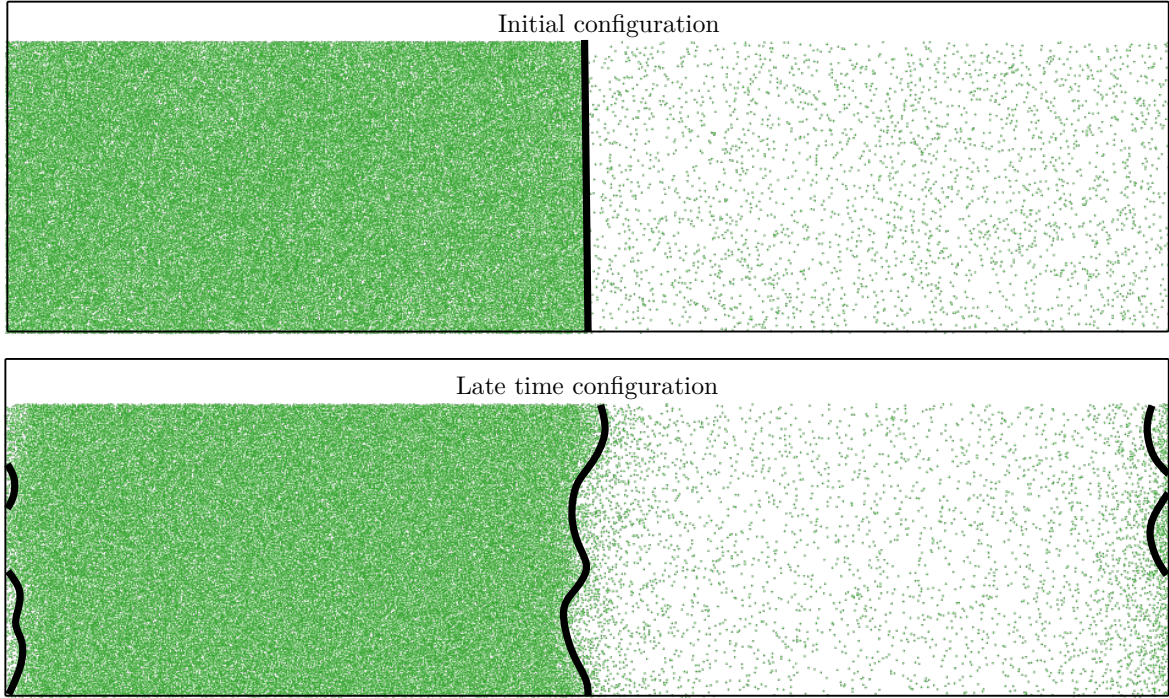


FIG. 4. Initial and late time configuration of a typical system.

We numerically integrate Eqs. (5) and (6) using an event-driven molecular dynamics algorithm [72], modified to include a Langevin bath via discrete-time kicks.

For simplicity, we first consider the case $T = 0$. In this regime, two particles i and j collide after a time:

$$\delta\tau_{ij}^{\text{coll}} = -\log(1 - \Gamma\delta\tau_{ij})/\Gamma \quad \text{with} \quad \delta\tau_{ij} = \frac{-b - \sqrt{b^2 - \mathbf{v}_{ij}^2(\mathbf{r}_{ij}^2 - (\sigma_i + \sigma_j)^2/4)}}{\mathbf{v}_{ij}^2}, \quad (9)$$

where $b = \mathbf{r}_{ij} \cdot \mathbf{v}_{ij}$ and \mathbf{r}_{ij} and \mathbf{v}_{ij} are respectively the relative position and velocity of particles i and j at the moment the subsequent collision time is computed.

At each collision, particle velocities are updated according to the energy change given in Eq. (6), leading to the post-collision velocities \mathbf{v}' :

$$\mathbf{v}'_i = \mathbf{v}_i - \frac{\mathbf{v}_{ij} \cdot \hat{\boldsymbol{\sigma}}_{ij} + \sqrt{\alpha^2(\mathbf{v}_{ij} \cdot \hat{\boldsymbol{\sigma}}_{ij})^2 + 4\Delta E^+}}{2} \boldsymbol{\sigma}_{ij} \quad \text{and} \quad \mathbf{v}'_j = \mathbf{v}_j + \frac{\mathbf{v}_{ij} \cdot \hat{\boldsymbol{\sigma}}_{ij} + \sqrt{\alpha^2(\mathbf{v}_{ij} \cdot \hat{\boldsymbol{\sigma}}_{ij})^2 + 4\Delta E^+}}{2} \boldsymbol{\sigma}_{ij}. \quad (10)$$

For $T \neq 0$, each particle receives stochastic kicks every δt_{noise} , drawn from a Gaussian distribution of variance $2\Gamma T \delta t_{\text{noise}}/m^2$ [100]. To properly resolve the dynamics, we require $\delta t_{\text{noise}} \ll \tau^{\text{coll}}$, where τ^{coll} is the mean free flight time between successive collisions.

Simulations are initialized at $t = 0$ with a flat interface and phase densities set to their homogeneous coexistence values previously obtained: $\phi_{t=0}(x, y) \simeq (\phi_{\text{dense}}^{\text{coexistence}} - \phi_{\text{dilute}}^{\text{coexistence}})\Theta(x - L_x/2) + \phi_{\text{dilute}}^{\text{coexistence}}$ (where Θ is the Heaviside function). The phases are initialized in their correct phases (ideal solid, amorphous or liquid) except for the case $\delta E_0/\hat{E} = 0.0054$ in Fig. 2 where we initialized the dense phase in a liquid while it slowly crystallized at $t > 0$. We kept this as an educative example, showing that a system with multiple hexatic domains behave similarly to a system with a unique and well oriented crystal. The total packing fraction $\phi = \pi\sigma^2 N/4L_x L_y$ is set such that the interface rests, on average, at $x = L_x/2$. Due to significant finite-size effects, these initial coexistence densities depend on the

system size and must be carefully tuned from preliminary simulations. The one-dimensional interface profile $h(y)$ is obtained by extracting the local packing fraction field $\phi(x, y)$ through binning via squares of length 5σ . The position of the interface $h(y)$ is placed by fitting each y -slice to a hyperbolic tangent: $\phi(x, y) = A \tanh[(x - h(y))/B] + C$. The interface coarsens with time and reaches a stationary regime at a time τ_{ss} which is numerically obtained by looking at the first time the average $W^2(L, t)$ reaches its stationary value $W^2(L, t \rightarrow \infty)$.

The initial and late time state of a typical system are illustrated in Fig. 4.

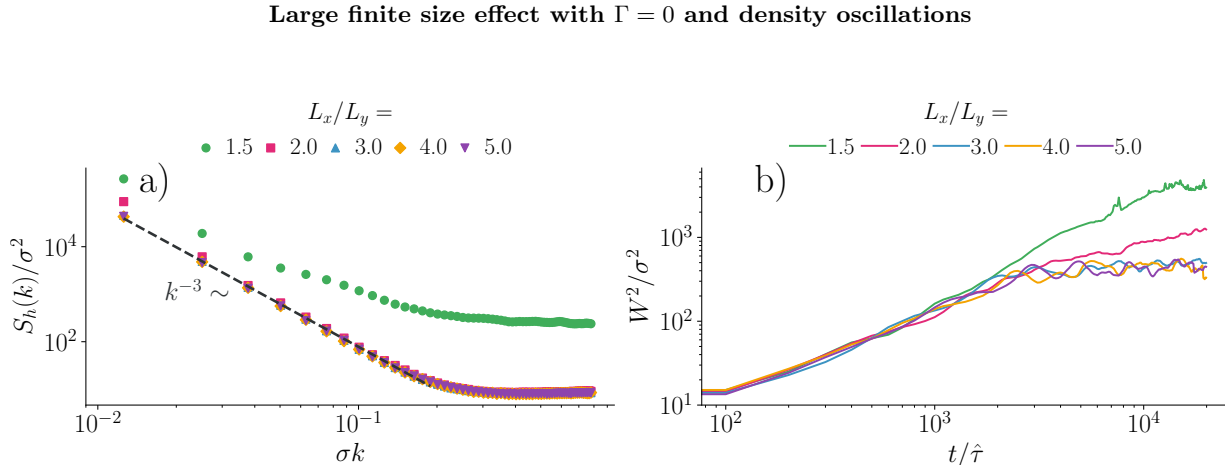


FIG. 5. Quantification of the finite size effects for the system with $\Gamma = 0$ and $L_y = 500\sigma$. a) Static height correlation function for various system size. b) Coarsening of these different system sizes with time. The parameters are the same as the one used in Fig. 1 of the main text for the system with $\Gamma = 0$.

To isolate bulk-driven interfacial fluctuations, the simulation box must be sufficiently long in the direction perpendicular to the interface [102], ensuring that the two interfaces do not interact. For systems with $\Gamma = 0$, finite-size effects become particularly severe. As shown in Fig. 5a) where L_x is varied for a fixed $L \equiv L_y$. S_h varies significantly for $L_x < 3L_y$. Correspondingly, Fig. 5b) shows anomalous coarsening dynamics in such undersized systems, with the interface roughness growing faster than in the largest system sizes. This issue worsens with increasing L_y as the critical aspect ratio L_x/L_y required to suppress finite-size artifacts also increases. Thus, larger interfaces demand even more elongated simulation boxes to reach the scaling regime. This result is perhaps not unexpected, as $\chi = 1$ marks the stability limit for an interface in the thermodynamic limit. Indeed, given the scaling $\sqrt{W_{ss}^2(L_y)} \sim L_y^\chi$, $\chi = 1$ implies the interface width increases proportionally to its base length. Consequently, for $\chi = 1 + \varepsilon$ (with $\varepsilon > 0$), the interface becomes unstable for a given $L_y = L'_y$ such that $W^2(L'_y) > L_x$, if the aspect ratio L_x/L_y is held fixed.

However, increasing L_x introduces two complications: the simulation time explodes and standing waves emerge. Indeed, Fig. 6a) reveals oscillations in the mean interface width, which become increasingly prominent with system size. These oscillations correspond to standing compressive waves in the density field, as shown in Fig. 6b.) They originate from the mismatch between our initial condition – a sharp flat interface – and the smooth mechanical equilibrium profile expected due to surface tension, which resembles a $\tanh(x/\zeta)$ interpolation between bulk phases. The resulting force imbalance at the phase boundaries launches compressive waves that decay only weakly in the absence of external damping ($\Gamma = 0$).

This effect appears negligible for interfaces involving solid or glassy phases. Nevertheless, for gas-liquid systems, these density waves dominate interfacial coarsening, masking the intrinsic scaling behavior at early time and making it impossible to extract z . The examples provided here are exaggerated by purposely initializing the density field with a relatively large density mismatch compared to the measured coexistence densities.

Coarsening of liquid-solid interfaces

Coarsening dynamics in systems undergoing liquid-solid phase separation are significantly more challenging to characterize than in liquid-gas systems. An accurate initialization is important: the solid phase should ideally be unstrained, for instance using a direct-coexistence protocol [101]. In this work, we did not implement such equilibra-

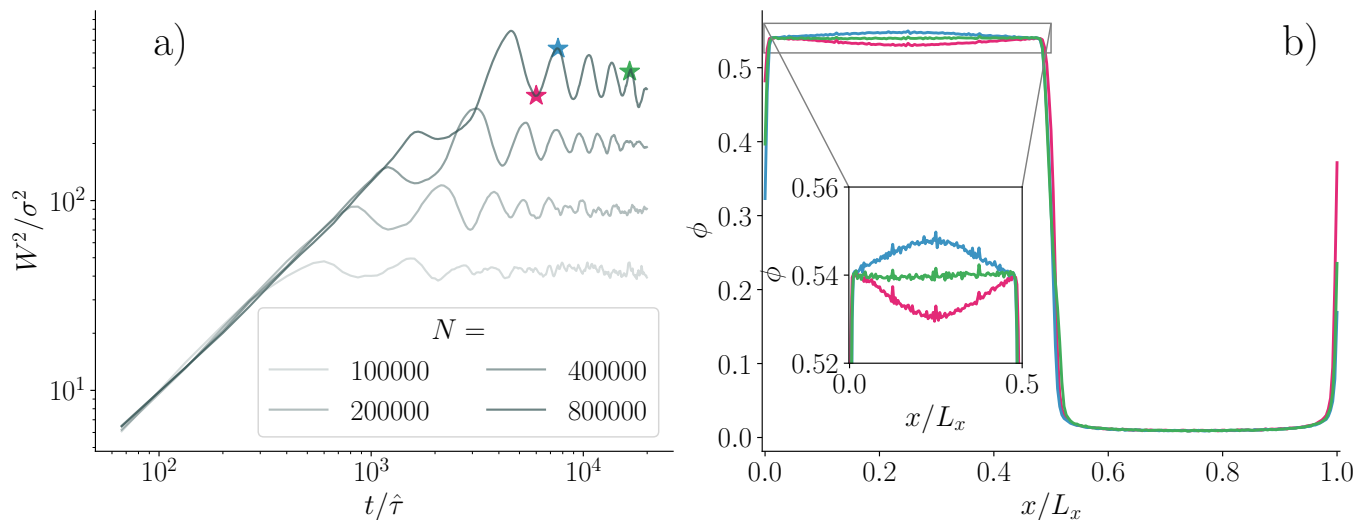


FIG. 6. Spurious oscillations due to initial force imbalance at the boundaries. a) Coarsening with respect to time for different system size. b) Density profile along the direction perpendicular to the interface at different time corresponding to the stars marked in a). The parameters are the same as the one used in Fig. 1 of the main text for the system with $\Gamma = 0$.

tion procedures, which may affect quantitative details of the observed coarsening. Nonetheless, we report here the qualitative trends across the different systems studied in the main text.

We first consider how coarsening changes as parameters are varied to induce crystallization of the dense phase.

The most pronounced changes are observed for $\Gamma = 0$, shown in Fig. 7a). For large δE_0 , the system remains in a liquid-gas regime and exhibits coarsening behavior similar to that discussed in the main text (note that we did not take any precaution to partially eliminate the spurious standing waves). As δE_0 is decreased, the dense phase begins to crystallize. Intermediate values produce systems with multiple hexatic domains that coarsen over time, as the initial state was roughly a disordered fluid at the same density. Interestingly, $W^2(t)$ becomes non-monotonic: the early-time increase corresponds to a predominantly liquid-gas interface, while the subsequent decrease reflects the formation of large hexatic domains that suppress interfacial fluctuations. We note that the W^2 becomes roughly constant at large time while the hexatic domains are still present and coarsening. We conclude that they coarsen slowly compared to the interface fluctuations. Further reduction of δE_0 yields a fully crystalline dense phase with markedly slower coarsening. For these systems, the dense phase was initialized with an ideal hexagonal solid.

In Fig. 7b), we provide the same figure but for the system following $|q|$ KPZ for the liquid-gas. Once again, crystallization leads to significantly reduced interface width. However, the coarsening phase at early time remains similar.

We now perform a finite-size analysis of systems with the smallest values of the control parameter, corresponding to the most densely packed solids.

We first consider the system with $\Gamma = 0$ (left-hand side of Fig. 8). As shown in Fig. 8a) and c), the interface coarsen in a manner that prohibits a clear extraction of z . The steady state W^2 can however be extracted and is given in panel b). The approximate logarithmic scaling suggests $\chi \simeq 0$. This trend is consistent with the height structure factor $S_h(k)$ shown in panel d), which predicts $0 \lesssim \chi \lesssim 0.15$.

In contrast, the system with $\Gamma \neq 0$ (right-hand side of the figure) shows more regular behavior. As seen in panel e), the coarsening appears well-behaved, and analysis of panels f) and g) yields estimates of $0 \lesssim \chi \lesssim 0.1$ and $z \simeq 2.25$.

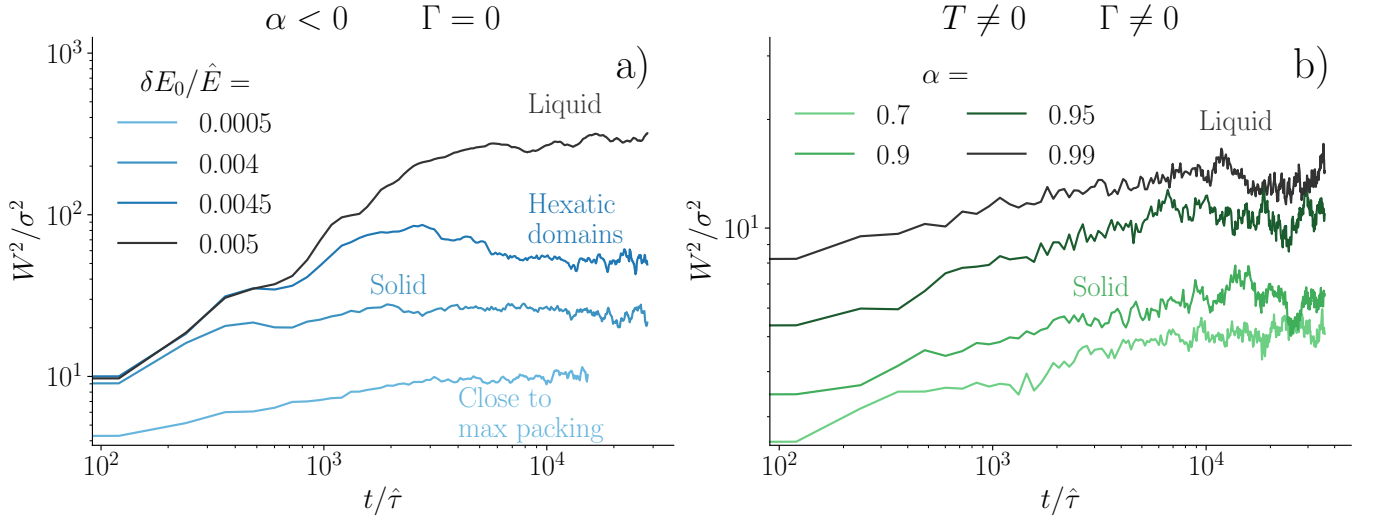


FIG. 7. Variation of the coarsening when the system changes from a liquid-gas to a liquid-solid phase separation. Left is a system with momentum conservation, right is without momentum conservation. The parameters are the same as the one used in Fig. 2

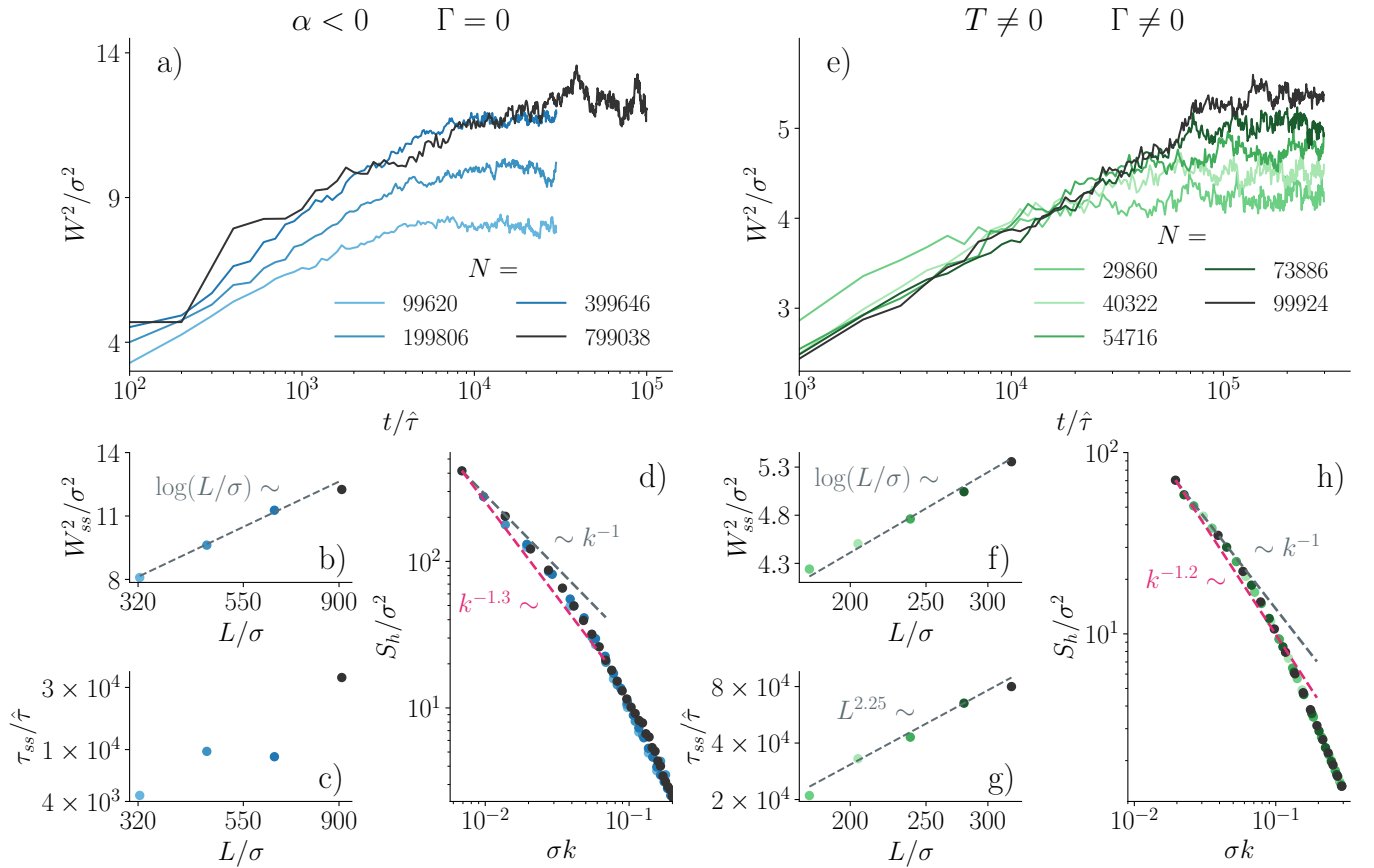


FIG. 8. Finite size analysis for the systems with a liquid-solid phase separation. Left is a system with momentum conservation and right is a system without. a) and e) are the evolution of the mean width squared as a function of L . b) and f) are the stationary values of W^2 as a function of L . c) and g) are the time required to reach this steady state value. d) and h) are the static height correlation in the steady state. For both systems, the parameters are the same as the ones used in Fig. 2 which lead to the densest glassy phase.